are an average over all multiplets arising from the ground-state configuration. The spin polarized method on the other hand does, in a way, distinguish between different multiplets.

Concerning the values obtained for the hardness, we notice that indeed larger values correspond to "harder" species. Therefore, metals are soft, according to the fact that chemical softness means little resistance of the chemical potential to change in the number of electrons. It is interesting to observe that among the four atomic properties calculated, hardness was the one that turned out to be the least sensitive to the functional model used. For the other three properties, the results are in general better for the Gunnarsson-Lundqvist approximation than for the X_α models, especially for heavier atoms, as it is expected for these models. But in most cases the error is small, typically less than 1 eV.

Certainly, major inaccuracies occur within the electron affinities, where in general the computed values underestimate the experimental values, especially those of the X_α approximation. This can be explained by the fact that eq 14 does not describe accurately the relaxation effects associated with the removal of an electron from the anion, since the orbitals employed in the calculation of χ and I are too contracted for this.

To obtain the best possible values, we should have included relativistic effects in the heavier atoms.[7] However, we feel that the uncertainty in the results due to the approximations to $E_{xc}[\rho]$ is the dominating error in our work. The selection of a more appropriate $E_{xc}[\rho]$ such as the SIC functional[23] should greatly improve the present results. Indeed this is what Whitehead has recently done.[24]

An exact exchange-correlation functional would give different numerical values, but most of these probably would not differ very much from the ones we have obtained. The main improvements would be expected to happen in the electron affinities values, especially in the negative ones.

Acknowledgment. We thank Professor Robert G. Parr for his encouragement and helpful comments about this work.

(23) Perdew, J. P.; Zunger, A. *Phys. Rev. B* **1981**, *23*, 5048.
(24) Whitehead, M. A., private communication.
(25) Nalewajski, R. F. *J. Am. Chem. Soc.* **1984**, *106*, 944.

Structurally Ordered Bimetallic One-Dimensional *catena*-μ-Dithiooxalato Compounds: Synthesis, Crystal and Molecular Structures, and Magnetic Properties of $AMn(S_2C_2O_2)_2(H_2O)_3 \cdot 4.5H_2O$ (A = Cu, Ni, Pd, Pt)

Alain Gleizes[†] and Michel Verdaguer*[‡]

Contribution from the Laboratoire de Chimie de Coordination du CNRS, 31400 Toulouse, France, and from the Laboratoire de Spectrochimie des Elēments de Transition, ERA No. 672, Universitē de Paris-Sud, 91405 Orsay, France. *Received September 27, 1983*

Abstract: Bimetallic one-dimensional compounds with dithiooxalato ($S_2C_2O_2^{2-}$) bridges were synthesized. Synthesis of $AMn(S_2C_2O_2)_2(H_2O)_3 \cdot 4.5H_2O$ with A = Cu (**1**), Ni (**2**), Pd (**3**), Pt (**4**) and crystal and molecular structures of **1**, **2**, and **4** are reported. All these compounds are isostructural and crystallize in the monoclinic system, space group $P2_1/c$, with four formula units per cell. Cell constants are as follows: **1**, a = 11.692 (2) Å, b = 20.665 (5) Å, c = 7.360 (2) Å, β = 103.84 (2)°; **2**, a = 11.575 (2) Å, b = 20.654 (5) Å, c = 7.323 (2) Å, β = 103.73 (2)°; **3**, a = 11.79 ± 0.02 Å, b = 20.78 ± 0.02 Å, c = 7.31 ± 0.02 Å, β = 103.5 ± 0.5°; **4**, a = 11.772 (4) Å, b = 20.806 (11) Å, c = 7.266 (3) Å, β = 103.52 (4)°. The structures consist of infinite chain molecules $\{[Mn(H_2O)_3](O_2C_2S_2)A(S_2C_2O_2)\}_\infty$ crisscrossing glide planes c and therefore stacked along these planes. Each layer of stacked chains is separated from the next one by intervening water molecules. The magnetic susceptibilities of the compounds are investigated in the temperature range 4.2-300 K. Compound **1** (Cu(II)-Mn(II)) is the first ferrimagnetic one-dimensional compound: it is made of alternating Cu(II) $^1/_2$ spins and Mn(II) $^5/_2$ spins antiferromagnetically coupled. The $\chi_M T$ vs. T curve shows a minimum at 130 K and a climb from 130 to 7.5 K; then three-dimensional ordering occurs as revealed by a decrease of $\chi_M T$ with T. The theoretical $\chi_M T$ vs. $kT/|J|$ curve (J = coupling constant between nearest neighbors) exhibits a minimum in the case of antiferromagnetic interaction, as observed in experimental results. The same feature appears in a theoretical model of alternating quantum spins $^1/_2$ and classical spins antiferromagnetically coupled. Both theoretical approaches are compared to experimental data, and values of J = -30.3 cm^{-1} and g = 1.90 are determined. An orbital interpretation of the interaction through dithiooxalato bridges between Cu(II) and Mn(II) ions is proposed.

Two years ago, we gave preliminary results about synthesis, structures, and magnetic data of a novel class of one-dimensional (1-D) compounds made of dithiooxalato ($S_2C_2O_2^{2-}$) bridges and pairs of Cu(II)-Mn(II) (**1**) and Ni(II)-Mn(II) (**2**) ions.[1] Synthesis and study of polynuclear complexes including 1-D systems are very active fields of inorganic chemistry and solid-state physics. Inorganic chemists try to synthesize new compounds and to predict their properties on the basis of a molecular approach to the exchange phenomenon,[2] whereas physicists test on 1-D materials the validity of phenomenological models using the Heisenberg-Dirac-Van Vleck Hamiltonian (HDVV).

In the last decade, both steps met noteworthy success in predicting magnetic properties or interpreting experimental data. On the one hand, useful structural magnetic correlations were established in the simplest binuclear units[3] or polynuclear ones;[4]

[†] Laboratoire de Chimie de Coordination du CNRS.
[‡] Laboratoire de Spectrochimie des Elēments de Transition.

(1) Gleizes, A.; Verdaguer, M. *J. Am. Chem. Soc.* **1981**, *103*, 7373-7374.
(2) (a) Hay, P. J.; Thibeault, J. C.; Hoffmann, R. *J. Am. Chem. Soc.* **1975**, *97*, 4884-4899. (b) Kahn, O.; Briat, B. *J. Chem. Soc., Faraday Trans. 2* **1976**, *7*, 268-281.
(3) (a) Crawford, V. H.; Richardson, H. W.; Wasson, J. R.; Hodgson, D. J.; Hatfield, W. E. *Inorg. Chem.* **1976**, *15*, 2107-2110. (b) Cline, S. J.; Hodgson, D. J.; Kallesoe, S.; Larsen, S.; Pedersen, E. *Ibid.* **1983**, *22*, 637-642 and references therein.
(4) Fletcher, R.; Hansen, J. J.; Livermore, J.; Willett, R. D. *Inorg. Chem.* **1983**, *22*, 330-334 and references therein.

0002-7863/84/1506-3727$01.50/0

orbital interpretation of exchange was proposed for both antiferromagnetic and ferromagnetic behavior,[5] and the first ab initio calculations on binuclear complexes of transition metals recently appeared.[6] On the other hand, agreement between theoretical HDVV approach and experimental results are often impressive.[7] Until our preliminary note, however, no one reported structurally characterized, ordered bimetallic chains of type $-(A-X-B-X-)_n$ where A and B are two different paramagnetic metal ions and X is a bridging ligand. Two years later, to the best of our knowledge, only one family of such compounds in addition to the present one was studied.[8] Of course, some 1-D bimetallic compounds have been known for a long time, but with only one magnetic ion in the chain ($HgCo(SCN)_4$). Likewise, 1-D homometallic materials with alternating interaction constants J_1 and J_2[9] and doped materials with statistical distributions of magnetic ions A in 1-D systems of ions B[10] have been studied.

For the first time, with **1** we have at hand an ordered chain of alternating ions with different numbers of unpaired electrons and a possible uniform J value.

It is a challenge for inorganic chemists to overcome kinetic and entropic hindrances to obtain such compounds. Metal ions and bridging ligands must be carefully chosen. Dissymmetric ligands seem most appropriate as they permit choosing coordinating atoms according to the nature of the metal ion to get stable compounds (hard–hard or soft–soft interactions, for example). From this point of view, dithiooxalato is a very versatile ligand which has a rich coordination chemistry with transition elements,[11] including rare-earth ions.[12]

In this paper, we report on the synthesis of $AMn(S_2C_2O_2)_2(H_2O)_3{\cdot}4.5H_2O$ with A = Cu (**1**), Ni (**2**), Pd (**3**), and Pt (**4**) and the crystal and molecular structures of **1**, **2**, and **4**. We reinvestigate the magnetic properties of **1**, which were rather deceiving in our first experiment, and we reveal the critical influence of the crystallization water molecules on structure and on properties. Actually **1** is the first ferrimagnetic macromolecular complex with antiferromagnetic interactions between Cu(II) and Mn(II) neighbors. The coupled neighboring spins do not compensate in the short-range order state where copper and manganese spins are antiparallel, giving rise to a minimum in the $\chi_M T$ vs. T curve. Different theoretical approaches are proposed to fit this peculiar experimental behavior, here or elsewhere.[13a] An orbital interpretation follows which explains the exchange pathway through dithiooxalato bridges.

Experimental Section

Synthesis. Potassium bis(dithiooxalato)nickelate(II) and -cuprate(II), $K_2Ni(S_2C_2O_2)_2$ and $K_2Cu(S_2C_2O_2)_2$, were prepared from potassium dithiooxalate (Eastman Kodak) as described in ref 14 and 15, respectively. $K_2Pd(S_2C_2O_2)_2$ and $K_2Pt(S_2C_2O_2)_2$ were prepared according to the same procedure as $K_2Ni(S_2C_2O_2)_2$ using K_2PdCl_4 and K_2PtCl_4 as palladium and platinum sources.

$CuMn(S_2C_2O_2)_2(H_2O)_3{\cdot}4.5H_2O$ (1) was prepared in aqueous medium by reacting a warm slurry of $K_2Cu(S_2C_2O_2)_2$ with a hot concentrated solution of manganese(II) sulfate in a twofold molar excess. The resulting solution was maintained at about 70 °C under stirring during a few minutes and then slowly cooled down to room temperature. The brown, ribbon-shaped crystals which formed were collected by suction filtration. They were washed several times with cold water and dried in a gentle stream of not too dry ambient air (vide infra). Yields were about 60%.

Anal.[16] Calcd for $CuMn(S_2C_2O_2)_2(H_2O)_{7.5}$: Mn, 11.12; Cu, 12.87; S, 25.97. Found: Mn, 10.58; Cu, 12.44; S, 24.07.

$AMn(S_2C_2O_2)_2(H_2O)_3{\cdot}4.5H_2O$ (A = Ni (2), Pd (3), Pt (4)) were prepared in a similar manner but with use of concentrated solutions instead of slurries. Here again, the crystals obtained are ribbon shaped. With nickel and platinum they are black, while those with palladium are orange.

Anal. Calcd for $NiMn(S_2C_2O_2)_2(H_2O)_{7.5}$: Mn, 11.23; Ni, 12.00; S, 26.22; C, 9.82; H, 3.09. Found: Mn, 11.24; Ni, 12.06; S, 26.32; C, 10.00; H, 2.82. Calcd for $PdMn(S_2C_2O_2)_2(H_2O)_{7.5}$: Mn, 10.23; Pd, 19.82; S, 23.89; C, 8.95; H, 2.82. Found: Mn, 10.23; Pd, 20.41; S, 23.37; C, 9.27; H, 2.74. Calcd for $PtMn(S_2C_2O_2)_2(H_2O)_{7.5}$: Mn, 8.78; Pt, 31.19; S, 20.51; C, 7.68; H, 2.42. Found: Mn, 9.05; Pt, 31.98; S, 21.14; C, 8.10; H, 1.97.

$CuMn(S_2C_2O_2)_2(H_2O)_3$ (5). When the crystals of $CuMn(S_2C_2O_2)_2(H_2O)_3{\cdot}4.5H_2O$ are dried under vacuum or in a silica gel dessiccator or in a warm atmosphere their color turns black and they deformate by twisting. The elemental analysis suggests the formula $CuMn(S_2C_2O_2)_2(H_2O)_3$. Anal. Calcd: Mn, 13.31; Cu, 15.39; S, 31.07. Found: Mn, 13.41; Cu, 15.50; S, 31.01.

X-ray Diffraction Studies. The isostructurality of the four compounds $AMn(S_2C_2O_2)_2(H_2O)_3{\cdot}4.5H_2O$ was first deduced from X-ray powder photographs taken with a Guinier camera using Mo Kα radiation. This study was tedious since the aspect of the powder patterns strongly depended on the strength of grinding but not in the same way from one compound to the other. Actually, the Cu derivative was found to transform more easily upon grinding than those of the d^8 ions.

From precession photographs taken with a Stoe camera using Mo Kα radiation, the four compounds were found to crystallize in the monoclinic system of space group $P2_1/c$ and to have nearly identical cell constants which were refined later on the diffractometer for the Cu, Ni, and Pt compounds (Table I).

It has not been possible to grow crystals thicker than 0.02 mm. The crystals were found to be very fragile and subject to spontaneous shrinking and twisting upon application of the slightest mechanical stress. To minimize the risk of such an event during X-ray measurements, the crystals were mounted laid on the wall of a Lindemann glass capillary

Table I. Physical and Crystallographic Data for the Series of Isomorphous Compounds $AMn(S_2C_2O_2)_2(H_2O)_3{\cdot}4.5H_2O$ (A = Cu, Ni, Pd, Pt)

	Cu[a]	Ni[a]	Pd[b]	Pt[a]
mol wt	493.90	489.07	536.76	625.45
color	dark brown	dark red	orange	black
a, Å	11.692 (2)[c]	11.575 (2)	11.79 ± 0.02	11.772 (4)
b, Å	20.665 (5)	20.654 (6)	20.78 ± 0.02	20.806 (11)
c, Å	7.360 (2)	7.323 (1)	7.31 ± 0.02	7.266 (3)
β, deg	103.84 (2)	103.73 (1)	103.5 ± 0.5	103.52 (4)
V, Å^3	1727	1701	1741	1730
ρ_{calcd}, g cm^{-3}	1.90	1.91	2.05	2.40
ρ_{expti}, g cm^{-3}	not dtd[d]	1.92 ± 0.02	not dtd[d]	not dtd[d]

[a] Cell constants were refined on the diffractometer by optimizing the settling angles of 25 reflections. [b] Cell constants were derived from precession photographs. [c] Estimated standard deviations in the last significant figure(s) in this and subsequent tables are given in parentheses. [d] Not determined.

(5) Kahn, O.; Charlot, M. F. *Nouv. J. Chim.* **1980**, *4*, 567–576.
(6) de Loth, P.; Cassoux, P.; Daudey, J. P.; Malrieu, J. P. *J. Am. Chem. Soc.* **1981**, *103*, 4007–4016.
(7) (a) Diederix, K. M.; Blöte, H. W. J.; Groen, J. P.; Klaasen, T. O.; Poulis, N. J. *Phys. Rev. B* **1979**, *B19*, 420–431. (b) Bonner, J. C.; Friedberg, S. A.; Kobayashi, H.; Meier, D. L.; Blöte, H. W. J. *Ibid.* **1983**, *B27*, 248–260.
(8) (a) Beltran, D.; Escriva, E.; Drillon, M. *J. Chem. Soc., Faraday Trans.* **1982**, *78*, 1773–1779. (b) Drillon, M.; Coronado, E.; Beltran, D.; Georges, R. *Chem. Phys.* **1983**, *79*, 449–453.
(9) Bonner, J. C.; Blöte, H. W. J.; Bray, J. W.; Jacobs, I. S. *J. Appl. Phys.* **1979**, *50*, 1810–1812.
(10) Dupas, C.; Renard, J. P.; Seiden, J.; Cheik-Rouhou, A. *Phys. Rev. B* **1982**, *B25*, 3261–3272.
(11) (a) Coucouvanis, D.; Baezinger, N. C.; Johnson, N. C. *J. Am. Chem. Soc.* **1973**, *95*, 3875–3881. Hollander, F. J.; Coucouvanis, D. *Inorg. Chem.* **1974**, *13*, 2381–2386. Leitheiser, M.; Coucouvanis, D. *Ibid.* **1977**, *16*, 1611–1614. Hollander, F. J.; Leitheiser, M.; Coucouvanis, D. *Ibid.* **1977**, *16*, 1615–1619. (b) Gleizes, A.; Clery, F.; Bruniquel, M. F.; Cassoux, P. *Inorg. Chim. Acta* **1976**, *37*, 19–26. (c) Maury, F.; Gleizes, A. *Ibid.* **1980**, *19*, 2074–2078. (d) Gleizes, A.; Maury, F.; Cassoux, P.; Galy, J. *Z. Kristallogr.* **1981**, *155*, 293–306. (e) Maury, F.; Gleizes, A. *C. R. Hebd. Séances Acad. Sci., Ser. C* **1980**, *291*, 49–52.
(12) Trombe, J. C.; Gleizes, A.; Galy, J. *C. R. Hebd. Séances Acad. Sci., Ser. C* **1982**, *294*, 1369–1372. Trombe, J. C.; Gleizes, A.; Galy, J. *Inorg. Chim. Acta*, in press.
(13) (a) Verdaguer, M.; Gleizes, A.; Renard, J. P.; Seiden, J. *Phys. Rev. B*, in press. (b) Such behavior could be attributed to zero-field splitting. But zfs is detectable neither in magnetization measurements in **1**[13a] nor in subsequent studies of the susceptibility in low field: for **1**, near 3-D ordering, the peak in $\chi_M = f(T)$ is very sharp (Renard, J. P., work in progress).
(14) Cox, E. G.; Wardlaw, W.; Webster, K. C. *J. Chem. Soc.* **1912**, 1475–1480.
(15) Pearson, R. G.; Sweigart, D. A. *Inorg. Chem.* **1970**, *9*, 1167–1175.
(16) Elemental analysis were performed at the Service Central de Microanalyse du C.N.R.S.

Table II. Experimental Crystallographic Data

	Ni compound	Cu compound
	1. Data Collection	
cryst dimens, cm	0.025 × 0.008 × 0.002	0.022 × 0.007 × 0.002
face indices	(100) (010) (001)	
absorption, μ, cm^{-1}	24.0	25.6
temp, K	293	
radiation	λ(Mo Kα) = 0.71069 Å	
crystal-detector dist, mm	208	
detector window		
height, mm	4	
width, mm	4	
take-off angle, deg	2.5	4
scan mode	θ–θ	θ–2θ
max Bragg angle, deg	30	33
scan angle		
$\Delta\theta = \Delta\theta_0 + B\mathrm{tg}\theta$	$\Delta\theta_0$[a] = 0.65	$\Delta\theta_0$ = 0.95
	B = 0.347	
values determining scan-speed		
Sigpre[a]	0.666	
Sigma[a]	0.018	
Vpre,[a] deg/min	10	
T_{max},[a] s	50	
controls		
intensity reflections	102, 122, 0100	020, 102, 112
periodicity	every 3600 s	
orientation		
reflections	0120, 1200, 214	0100, 1200, 214
periodicity	every 100 reflections	
	2. Conditions for Refinement	
recorded reflcns	3664	6381
independent reflcns	3159	6133
utilized reflcns	894 ($I > 1.5\sigma(I)$)	1149 ($I > 2\sigma(I)$)
refined parameters	120	155
reliability factors R	0.059	0.064
R_w	0.053	0.057

[a] These parameters have been described by: Mosset, A.; Bonnet, J.-J.; Galy, J. *Acta Crystallogr., Sect. B*, **1977**, *B33*, 2633.

previously covered with a thin layer of grease. In the case of the copper compound which easily loses water, the crystal was mounted wet in the capillary.

Diffracted intensities were measured on a CAD-4 Enraf-Nonius, PDP8/M computer-monitored diffractometer using Mo Kα radiation. The data collection conditions for the Cu and Ni compounds are presented in Table II. Due to the fragility of the crystals, data had to be collected quite rapidly, and only reflections corresponding to Miller indices *hkl* and *hkl̄* were measured. For the Ni compound, the collection could not be completed since the crystal "died out" suddenly without any premonitory anomalies in standard intensities. For the Cu compound, the standards showed no abnormal trends. The data were processed[17] with use of an ignorance factor p of 0.01 for the Cu compound and of 0.02 for the Ni compound in the estimation of standard deviations. No absorption corrections were applied. Thinness of the crystals made unavailable the necessary number of significant intensities above background to allow comfortable structure determinations. However, our results were accurate enough for the purpose of relating physical properties with structural features.

The case of the Pt compound will be handled below.

Crystal Structure Determinations. The structure determinations were carried out by using Patterson and Fourier map techniques and the refinements by applying full-matrix least-squares techniques. Throughout the refinement the function minimized was $\sum w(F_o - |F_c|)^2$, where F_o and $|F_c|$ are the observed and calculated structure amplitudes. The reliability factors are defined as $R = \sum||F_o| - |F_c||/F_o$ and $R_w = \{\sum w(F_o - |F_c|)^2/\sum wF_o^2\}^{1/2}$. The atomic scattering factors and anomalous terms (metals and sulfur atoms) are those of Cromer and Waber.[18]

Table III. Positional Parameters for the Atoms of $CuMn(S_2C_2O_2)_2(H_2O)_3 \cdot 4.5H_2O$

atom	x	y	z
atom	x	y	z
Mn	0.78765 (29)	0.35115 (13)	0.4558 (5)
S(1)	0.1061 (4)	0.29824 (28)	0.1394 (8)
S(2)	0.2086 (4)	0.1508 (3)	0.1660 (9)
S(3)	0.4690 (4)	0.20405 (29)	0.2853 (9)
S(4)	0.3686 (4)	0.35197 (28)	0.2366 (9)
O(1)	0.9013 (10)	0.2614 (7)	0.5325 (18)
O(2)	0.9847 (10)	0.3793 (1)	0.5553 (19)
O(3)	0.6711 (10)	0.2620 (7)	0.3741 (20)
O(4)	0.5905 (11)	0.3810 (8)	0.3328 (20)
C(1)	0.0125 (16)	0.2343 (10)	0.0826 (26)
C(2)	0.0608 (16)	0.1674 (9)	0.0995 (27)
C(3)	0.5611 (16)	0.2673 (9)	0.3250 (26)
C(4)	0.5189 (17)	0.3375 (10)	0.3061 (29)
Ow(1)	0.7574 (10)	0.3468 (7)	0.7317 (17)
Ow(2)	0.8155 (10)	0.3530 (7)	0.1754 (18)
Ow(3)	0.7863 (11)	0.4557 (5)	0.4683 (21)
Ow(4)	0.0431 (12)	0.4716 (7)	0.2869 (19)
Ow(5)	0.4245 (13)	0.4691 (8)	0.5945 (22)
Ow(6)	0.1331 (14)	0.4582 (8)	0.9638 (22)
Ow(7)	0.7070 (12)	0.4469 (8)	0.9369 (21)
Ow(8)[a]	0.479 (3)	0.4743 (16)	0.955 (5)

[a] Half-occupied positions.

$NiMn(S_2C_2O_2)_2(H_2O)_3 \cdot 4.5H_2O$. The positions of the Ni and Mn atoms were derived from the Patterson map and their refinement along with the scale factor yielded R = 0.48. An ensuing Fourier map permitted location of atoms of dithiooxalate groups. An isotropic refinement resulted in R = 0.25 and R_w = 0.30. Next were found positions of water molecules bound to manganese; their introduction in the refinement gave R = 0.18 and R_w = 0.22. The following difference Fourier maps exhibited peaks which were attributed to isolated water molecules which were progressively placed. Due to the lack of data, anisotropic thermal coefficients were introduced only for the metal and sulfur atoms. Hydrogen atoms could not be really localized. Convergence was achieved with R = 0.059 and R_w = 0.053 using 894 reflections with $I > 1.5\sigma(I)$ for 120 variables. In the last cycle of refinement, variable shifts were less than 5% of estimated standard deviations; the error in an observation of unit weight was 2.16 e. The final difference Fourier map did not show peaks higher than one-eighth of the peaks corresponding to carbon atoms on the Fourier map. Refined atomic positions are listed in Table III.[38]

$CuMn(S_2C_2O_2)_2(H_2O)_3 \cdot 4.5H_2O$. The positions found in the previous structure for the metal atoms, the dithiooxalate groups atoms, and the water molecules bound to manganese were introduced in the least-squares calculation and refined isotropically along with the scale factor. The reliability factors fixed at R = 0.18 and R_w = 0.22. An ensuing difference Fourier map yielded the isolated water molecules at the same positions as in the Ni compound. Anisotropic thermal parameters were introduced for metal and sulfur atoms and oxygen atoms bound to metals. In the last cycle of refinement (variable shift)/(estimated standard deviation) ratios were less than 12%. The reliability factor stabilized at R = 0.064 and R_w = 0.057 for 1149 reflections having $I > 2\sigma(I)$ and 155 variables. The error in an observation of unit weight was 2.52 e. The final difference Fourier map was featureless. Refined atomic positions are listed in Table IV.[38]

$PtMn(S_2C_2O_2)_2(H_2O)_3 \cdot 4.5H_2O$. A crystal of the Pt compound was found to have a monoclinic cell differing from that of the Ni and Cu derivatives; it was at first thought to be representative of a new variety. The intensities were measured, and in the course of the structure determination it turned out that the crystal was twinned. However, the crystal structure could be established accurately enough, but the work is not yet entirely completed (R = 0.066, R_w = 0.073). Therefore, interatomic distances, angles, and mean planes given below are just presented for comparison with those of the Ni and Cu compounds. The complete structure solution from the twin will be published later.

(17) All X-ray structure calculations were performed with use of the CII Iris-80 computer of the Centre Interuniversitaire de Calcul de Toulouse. The following programs were employed: Aussoleil and Legros' CAD 4-CICT 10, a local program for data reduction; Zalkin's FORDAP Fourier summation program; Ibers' NUCL full-matrix least-squares program, which in its nongroup version resembles Busing and Levy's ORFLS program; Johnson's ORTEP thermal ellipsoid plotting program; Busing and Levy's ORFFE error function program; Ahmed's NRC 22 least-squares plane program.

(18) "International Tables for X-ray Crystallography"; Kynoch Press: Birmingham, England, 1974; Vol. IV, Table 2.2 A (Cromer, D. T.; Waber, J. T.); Table 2.3.1 (Cromer, D. T.).

Table IV. Positional Parameters for the Atoms of $NiMn(S_2C_2O_2)_2(H_2O)_3 \cdot 4.5H_2O$

atom	x	y	z
Ni	0.28599 (22)	0.25137 (13)	0.2066 (4)
Mn	0.78659 (28)	0.35121 (11)	0.4533 (4)
S(1)	0.1113 (4)	0.29615 (23)	0.1397 (7)
S(2)	0.2106 (4)	0.15485 (23)	0.1701 (7)
S(3)	0.4607 (4)	0.20595 (23)	0.2772 (7)
S(4)	0.3619 (4)	0.34839 (23)	0.2354 (7)
O(1)	0.9028 (10)	0.2600 (5)	0.5323 (1)
O(2)	0.9865 (10)	0.3785 (6)	0.5560 (15)
O(3)	0.6707 (11)	0.2615 (5)	0.3723 (17)
O(4)	0.5849 (10)	0.3809 (6)	0.3262 (16)
C(1)	0.0168 (16)	0.2347 (8)	0.0861 (22)
C(2)	0.0619 (16)	0.1682 (8)	0.0977 (24)
C(3)	0.5595 (18)	0.2678 (8)	0.3210 (25)
C(4)	0.5098 (17)	0.3370 (8)	0.3005 (25)
Ow(1)	0.7572 (10)	0.3474 (6)	0.7274 (16)
Ow(2)	0.8167 (10)	0.3515 (6)	0.1763 (16)
Ow(3)	0.7863 (11)	0.4569 (5)	0.4643 (18)
Ow(4)	0.0426 (11)	0.4725 (6)	0.2880 (16)
Ow(5)	0.4213 (12)	0.4676 (7)	0.5914 (19)
Ow(6)	0.1310 (13)	0.4569 (7)	0.9664 (20)
Ow(7)	0.7078 (13)	0.4508 (7)	0.9342 (20)
Ow(8)[a]	0.475 (3)	0.4740 (15)	0.965 (5)

[a] Half-occupied positions.

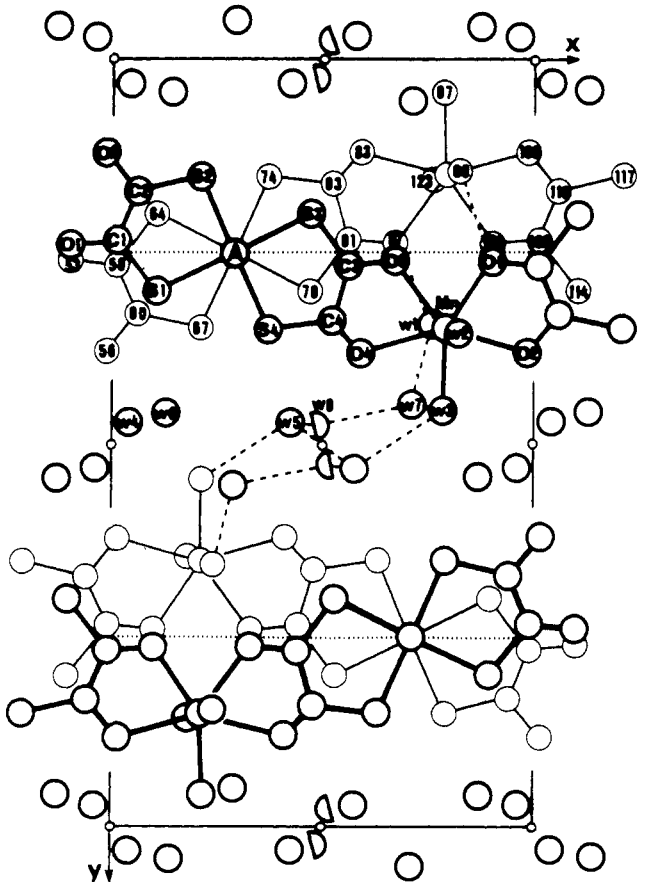

Figure 1. Ball and spoke drawing of the structure of $AMn(H_2O)_3(S_2C_2O_2)_2 \cdot 4.5H_2O$ (A = Cu, Ni, Pd, Pt) in projection onto the (001) plane. Glide planes c and centers of inversion are represented with conventional crystallographic symbols.

Susceptibility Measurements. The susceptibility measurements were performed on a Faraday balance equipped with a continuous-flow helium cryostat, already described.[19] The samples weighed typically 5–7 mg.

The products being sensitive to water loss (see Synthesis section) the samples were just degassed at 240 K during a few minutes to free the sample compartment of paramagnetic oxygen without destroying the compounds. Measurements were made under helium.

(19) Charlot, M. F.; Jeannin, S.; Jeannin, Y.; Kahn, O.; Lucrece-Abaul, J.; Martin Frere, J. *Inorg. Chem.* **1979**, *18*, 1675–1681.

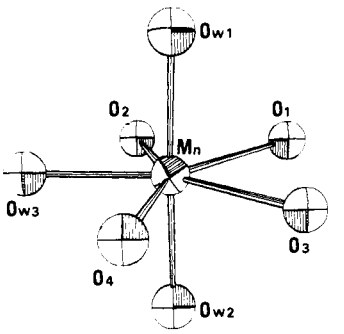

Figure 2. Coordination geometry of the Mn atom.

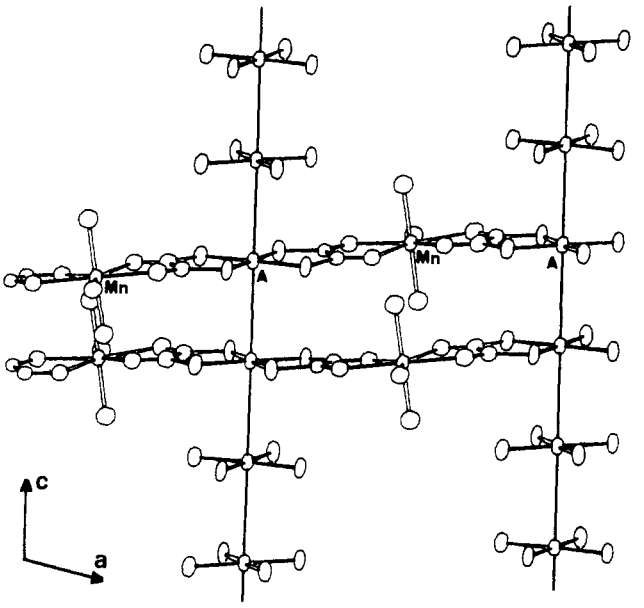

Figure 3. Partial view down the b axis of a layer of stacked ...A-$(S_2C_2O_2)$-$Mn(H_2O)_3$-$(O_2C_2S_2)$... chains, emphasizing the columnar structure generated by the AS_4 fragments.

Discussion of the Structures

The three compounds are isostructural. Their structures are made of extended zigzag chains ...$A(S_2C_2O_2)Mn(H_2O)_3(O_2C_2S_2)A$... (A = Cu, Ni, Pt) stacking along and crisscrossing glide planes c and of isolated water molecules. There are four unit formula $AMn(S_2C_2O_2)_2(H_2O)_3 \cdot 4.5H_2O$ per cell, the noninteger water content resulting from a water oxygen atom, Ow(8), half occupying a position very close to a center of inversion. A ball and spoke drawing of the structure projected along the c axis is given in Figure 1 with the numbering scheme of atoms. Interatomic distances are listed for the three compounds in the same table (Table V) for the sake of easy comparison.

Atom-to-plane distances and dihedral angles are presented in Table VI.[39] A short description of the structure illustrated with a stereoview of the cell has appeared.[1]

The A atoms are planarily tetracoordinated to the sulfur atoms S(1), S(2), S(3), S(4) of two dithiooxalato groups. The manganese atoms are heptacoordinated to oxygen atoms located at the vertices of a pentagonal bipyramid (Figure 2): four of these, O(1), O(2), O(3), O(4), belong to two dithiooxalate groups and the three other ones, Ow(1), Ow(2), Ow(3), are from water molecules. The AS(1)S(2)S(3)S(4) entity, the MnO(1)O(2)O(3)O(4)Ow(3) entity, and the dithiooxalate groups are quasi-planar, with mean planes making angles of about 4.5° on the average with each other and angles of about 1.5° with the b axis (Table VI). Therefore, within the chains, atoms (except Ow(1) and Ow(2)) form flat ribbons quasi-perpendicular to glide planes. These ribbons are nearly parallel to crystallographic planes $(10\bar{2})$.

Table V. Bond Lengths (Å) and Angles in $AMn(S_2C_2O_2)_2(H_2O)_3 \cdot 4.5H_2O$ (A = Ni, Pt, Cu)

	A = Ni	A = Pt	A = Cu
Around A			
A-S(1)	2.171 (5)	2.304 (10)	2.269 (6)
A-S(2)	2.167 (5)	2.287 (12)	2.272 (7)
A-S(3)	2.178 (5)	2.301 (11)	2.288 (6)
A-S(4)	2.178 (5)	2.296 (12)	2.267 (6)
S(1)-A-S(2)	92.2 (2)	90.1 (4)	91.9 (2)
S(1)-A-S(3)	179.2 (6)	177.8 (6)	178.0 (3)
S(1)-A-S(4)	87.8 (2)	90.1 (4)	89.1 (2)
S(2)-A-S(3)	87.6 (2)	89.4 (4)	87.7 (2)
S(2)-A-S(4)	178.5 (4)	178.6 (6)	177.5 (3)
S(3)-A-S(4)	92.5 (2)	90.4 (4)	91.5 (2)
Around Mn			
Mn-O(1)	2.31 (1)	2.30 (4)	2.27 (1)
Mn-O(2)	2.33 (1)	2.29 (2)	2.32 (1)
Mn-O(3)	2.29 (1)	2.25 (3)	2.29 (1)
Mn-O(4)	2.38 (1)	2.37 (3)	2.35 (1)
Mn-Ow(1)	2.12 (1)	2.26 (4)	2.14 (1)
Mn-Ow(2)	2.14 (1)	2.12 (3)	2.17 (1)
Mn-Ow(3)	2.18 (1)	2.18 (2)	2.16 (1)
Ow(1)-Mn-O(1)	87.0 (4)	87.7 (12)	87.1 (5)
Ow(1)-Mn-O(3)	90.0 (5)	91.5 (11)	89.6 (5)
Ow(1)-Mn-O(4)	91.0 (5)	91.0 (12)	90.4 (5)
Ow(1)-Mn-Ow(3)	90.0 (5)	88.7 (12)	89.8 (6)
Ow(1)-Mn-O(2)	94.2 (4)	97.0 (11)	95.0 (5)
Ow(2)-Mn-O(1)	91.3 (5)	93.5 (11)	92.3 (5)
Ow(2)-Mn-O(3)	88.5 (5)	87.5 (11)	88.8 (5)
Ow(2)-Mn-O(4)	89.7 (4)	87.1 (11)	89.2 (5)
Ow(2)-Mn-Ow(3)	92.0 (5)	91.1 (12)	91.6 (6)
Ow(2)-Mn-O(2)	86.1 (4)	84.8 (11)	86.1 (5)
O(1)-Mn-O(3)	70.9 (4)	72.6 (8)	71.6 (3)
O(3)-Mn-O(4)	69.3 (4)	69.2 (9)	69.0 (5)
O(4)-Mn-Ow(3)	75.3 (5)	74.2 (10)	74.8 (5)
Ow(3)-Mn-O(2)	75.9 (4)	76.8 (10)	75.7 (5)
O(2)-Mn-O(1)	69.0 (4)	68.0 (10)	69.4 (5)
Ow(1)-Mn-Ow(2)	178.0 (4)	178.1 (15)	178.4 (5)

	A = Ni	A = Pt	A = Cu
Dithiooxalate Ligand			
C(1)-S(1)	1.66 (2)	1.65 (3)	1.70 (2)
C(2)-S(2)	1.70 (2)	1.63 (4)	1.71 (2)
C(3)-S(3)	1.69 (2)	1.78 (4)	1.67 (2)
C(4)-S(4)	1.68 (2)	1.73 (4)	1.73 (2)
C(1)-O(1)$^{(i)\,a}$	1.29 (2)	1.33 (4)	1.27 (2)
C(2)-O(2)$^{(i)\,a}$	1.29 (2)	1.36 (5)	1.30 (2)
C(3)-O(3)	1.26 (2)	1.24 (4)	1.25 (2)
C(4)-O(4)	1.24 (2)	1.28 (4)	1.21 (2)
C(1)-C(2)	1.46 (2)	1.42 (5)	1.49 (2)
C(3)-C(4)	1.54 (2)	1.48 (5)	1.53 (2)
A-S(1)-C(1)	104.7 (6)	101.7 (12)	103.7 (7)
A-S(2)-C(2)	103.8 (6)	100.4 (17)	101.7 (7)
A-S(2)-C(2)	103.8 (6)	100.4 (17)	101.7 (7)
A-S(2)-C(2)	103.8 (6)	100.4 (17)	101.7 (7)
A-S(2)-C(2)	103.8 (6)	100.4 (17)	101.7 (7)
A-S(2)-C(2)	103.8 (6)	100.4 (17)	101.7 (7)
A-S(2)-C(2)	103.8 (6)	100.4 (17)	101.7 (7)
A-S(2)-C(2)	103.8 (6)	100.4 (17)	101.7 (7)
A-S(2)-C(2)	103.8 (6)	100.4 (17)	101.7 (7)
C(1)-C(2)-O(2)$^{(i)\,a}$	119.4 (14)	114 (3)	116.4 (16)
S(3)-C(3)-C(4)	117.7 (16)	120 (3)	123.0 (15)
S(3)-C(3)-O(3)	125.1 (14)	123 (3)	123.6 (15)
O(3)-C(3)-C(4)	117.2 (17)	117 (4)	113.4 (18)
S(4)-C(4)-C(3)	119.3 (15)	121 (3)	118.2 (15)
S(4)-C(4)-O(4)	124.9 (14)	121 (3)	122.1 (17)
O(4)-C(4)-C(3)	115.7 (18)	117 (4)	119.5 (18)
Intermolecular Contacts			
Ow(1)-O(3)$^{(i)\,a}$	2.77 (2)	2.71 (4)	2.77 (2)
Ow(2)-O(1)$^{(ii)\,a}$	2.81 (2)	2.89 (5)	2.87 (2)
Ow(1)-Ow(7)	2.76 (2)	2.63 (5)	2.71 (2)
Ow(2)-Ow(7)$^{(iii)\,a}$	2.81 (2)	2.76 (5)	2.72 (2)
Ow(3)-Ow(4)$^{(iv)\,a}$	2.76 (2)	2.79 (4)	2.79 (2)
Ow(3)-Ow(5)$^{(iv)\,a}$	2.81 (2)	2.89 (5)	2.86 (2)
Ow(4)-Ow(6)$^{(iii)\,a}$	2.80 (2)	2.86 (5)	2.82 (2)
Ow(4)-Ow(6)$^{(v)\,a}$	2.80 (2)	2.73 (5)	2.84 (2)
Ow(5)-Ow(5)$^{(iv)\,a}$	2.84 (3)	2.78 (7)	2.80 (3)
Ow(5)-Ow(8)	2.66 (4)	2.47 (9)	2.58 (4)
Ow(6)-Ow(7)$^{(vi)\,a}$	2.65 (2)	2.73 (6)	2.69 (2)
Ow(7)-Ow(8)	2.80 (4)	2.90 (9)	2.76 (4)

[a] Roman numeral superscripts refer to the following equivalent positions relative to x, y, z: (i) $x, {}^1/_2 - y, {}^1/_2 + z$; (ii) $x, {}^1/_2 - y, -{}^1/_2 + z$; (iii) $x, y, z - 1$; (iv) $1 - x, 1 - y, 1 - z$; (v) $\bar{x}, 1 - y, 1 - z$; (vi) $1 - x, 1 - y, 2 - z$.

The A atoms have their y coordinates very close to $^1/_4$ and therefore lie quite on the glide planes (y = 0.2518 (2), 0.2514 (1), and 0.2516 (2) for Cu, Ni, and Pt, respectively). The manganese atoms stand back at about 2 Å from each side of these planes. The chains are thus stacked into layers along the glide planes with the planar AS_4 fragments forming piles in which two successive entities are staggered by about 45°. This is emphasized on Figure 3. Along a pile the A-A spacings are practially equal to $c/2$. This is also the distance between mean planes of two successive AS_4 groups since they make angles of only about 1° with the vector joining two neighboring A atoms. This way of stacking is different from that observed in the alkali salts of $Ni(S_2C_2O_2)_2^{2-}$ [11b,c] and of $Cu(S_2C_2O_2)_2^{2-}$ [20] where the planar anions stack inclined on the stacking axis and the successive AS_4 entities eclipse each other. In $BaNi(S_2C_2O_2)_2 \cdot 6H_2O$,[11d] the anions are perpendicular to the stacking axis but the Ni atoms are out of it.

Besides the ordered distribution of the two kinds of metal atoms along chains, the most striking feature of this structure is that the chains are rather isolated from each other either within a stack or from one layer to the next one. Due to the presence of a glide plane within a layer of stacked chains, the closest interchain distances between ribbon atoms are larger than or equal to $c/2$, i.e., about 3.6–3.7 Å. As only the A atoms are aligned along the stacking axis (Figure 3) and since the highest van der Waals radius for nonmetals is here that of sulfur, 1.85 Å,[21] there are no marked van der Waals contacts between atoms from neighboring ribbons: the shortest interchain sulfur–sulfur distance exceeds 3.9 Å. Only water oxygen atoms Ow(1) and Ow(2), which stand out of ribbon plane, are in van der Waals contacts with atom O(3) of the above chain and atom O(1) of the below chain respectively (Figure 1): the corresponding distances range from 2.71 (4) to 2.87 (2) Å (Table V), which compare fairly well with twice the oxygen van der Waals radius of 1.40 Å.[21] Whether these bonds involve hydrogen atoms is most likely but cannot be argued since hydrogen atoms were not localized. The spacing of 3.6–3.7 Å also precludes noticeable interactions between overlapping π systems of dithiooxalate ligands.

The layers of stacked chains are separated by layers of inserted water molecules which prevent direct interstack contacts. However, oxygen–oxygen distances of nearly twice the van der Waals radius of oxygen exist between water molecules both coordinated to manganese and isolated (Table V) so that chain layers are related through a weak network of van der Waals contacts and/or hydrogen bonds involving water molecules only (Figure 1). The weakness and rarity of interaction between the successive layers

(20) Legros, J. P.; Girerd, J. J., private communication.

(21) Pauling, L. "The Nature of the Chemical Bond", 3rd ed.; Cornell University Press: Ithaca, NY, 1960.

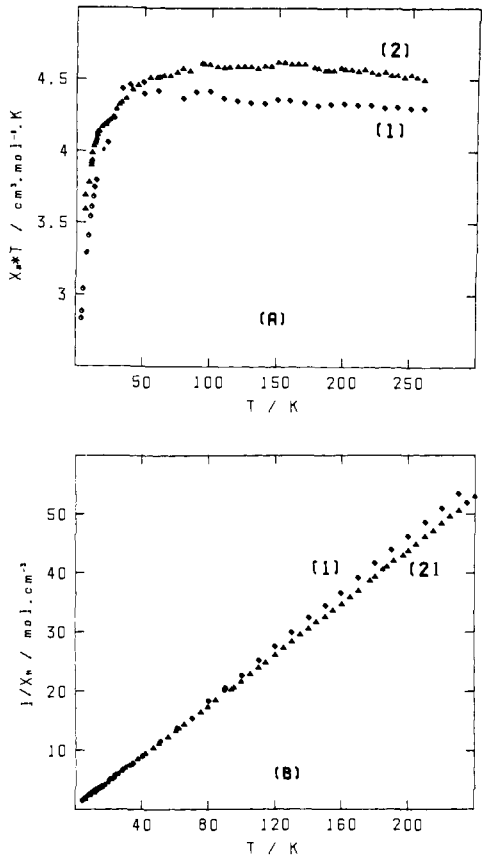

Figure 4. Experimental temperature dependence of the molar susceptibility for **2** (curve 1, ◇) and **3** (curve 2, △). (A) $\chi_M T$ vs. T. (B) χ_M^{-1} vs. T. (The molar weight chosen is given in the text.)

account for the fragility of compounds which easily lose the intercalated water molecules, yielding, for instance, the dehydrated Mn–Cu derivative mentioned in the preparative section. As dehydration results in twisted crystals no longer suitable for X-ray single-crystal techniques, EXAFS experiments are currently under way.

Bond lengths and angles show no unusual features and compare quite well with the values reported for $K_2Cu(S_2C_2O_2)_2$[20] and for the alkali,[11b,c] barium,[11d] and zinc[11e] salts of $Ni(S_2C_2O_2)_2^{2-}$ around the metal atoms and in the ligand as well.

Magnetic Behavior

The magnetic properties of the compounds are sketched in Figure 4 for compounds **2** and **3** and in Figure 5 for compounds **1** and **5**. The molecular weight is that of a binuclear unit, given in the Experimental Section. The curves of the nickel (**2**) and palladium (**3**) derivatives are close to each other, as can be expected for chains of manganese(II) ions far away from each other ($d_{Mn\text{-}Mn}$ intrachain $\simeq$ 12 Å and $d_{Mn\text{-}Mn}$ interchain $\simeq$ 5.6 Å). $\chi_M T$ is nearly constant in a large range of temperature (50–240 K) and then decreases rapidly (Figure 4a). The plots of χ_M^{-1} vs. T (Figure 4b) allow the determination of the Curie constant C at high temperature: 4.29 for **2** and 4.39 for **3** ($cm^3\ mol^{-1}\ K$) and the Curie–Weiss constant θ at low temperature

$$\chi_M = \frac{C}{T - \theta} \tag{1}$$

θ = −2.5 for **2** and −1.8 K for **3**. We attribute this behavior to weak antiferromagnetic coupling between manganese ions which can be assigned mainly to interchain coupling.[13b] In the mean-field approximation

$$\theta = \frac{2zJ'S(S+1)}{3} \tag{2}$$

(z is the number of nearest neighbors (2), J' is the coupling constant, and S is the manganese(II) spin = $^5/_2$). We find J' = −0.15 cm^{-1} (0.21 K) for **2** and −0.11 cm^{-1} (0.16 K) for **3**: the interchain coupling is weak in both cases.

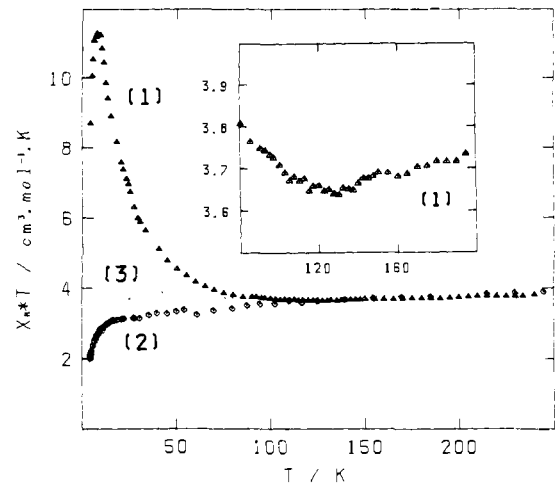

Figure 5. Experimental temperature dependence of the molar susceptibility as $\chi_M T$ vs. T for **1** (curve 1, △), **5** (curve 2, ◇), and partially dehydrated material **1** (see text) (curve 3, •).

We focus now on the magnetic behavior of the copper derivative **1** (Figure 5). The main feature is the existence of a minimum at 130 K, where $\chi_M T$ = 3.64 $cm^3\ mol^{-1}$ K, and a sharp increase between 130 and 7.5 K. In the temperature range 55–9 K, χ_M varies as $T^{-1.57}$. Below the temperature of the maximum, at 7.5 K, $\chi_M T$ rapidly decreases. A first interpretation may be as follows: copper(II), spin $^1/_2$, and manganese(II), spin $^5/_2$, are antiferromagnetically coupled through the dithiooxalato anion. At high temperatures, the paramagnetic limit is reached, when kT overcomes J, the intrachain coupling constant in the Hamiltonian

$$\mathcal{H} = -J\sum_{i=1}^{N}(\hat{S}_{2i-1}\hat{S}_{2i} + \hat{S}_{2i}\hat{S}_{2i+1}) \tag{3}$$

($\hat{S}_i = \hat{S}_{i+2} = \hat{S}_{Cu}$; $\hat{S}_{i+1} = \hat{S}_{i+3} = \hat{S}_{Mn}$; $\hat{S}_i$ are spin operators; N is the number of pairs). The minimum corresponds to a short-range order state where the copper spins are antiparallel to the manganese ones, without significant correlations between neighboring manganese ions. When the temperature decreases, the correlation length in the chain increases, leading to a ferrimagnetic short-range order. The sudden decrease around 7.5 K may be interpreted by a three-dimensional (3-D) ordering as a consequence of antiferromagnetic coupling between the chains (as already pointed out in isostructural compounds **2** and **3**).

Magnetization measurements performed at 1.3 and 4.2 K corroborate this analysis.[13a] The picture is complicated, however, by weak ferromagnetism due to spin canting. The above arguments give nevertheless a qualitative explanation of the main features of the magnetic properties of this *first ferrimagnetic quasi-one-dimensional material.*

The increase of $\chi_M T$ in a large temperature range (130–7.5 K) is allowed because the compound is a rather good 1-D chain ($|J'|$ interchain $\ll |J|$ intrachain). With a larger $|J'|$, 3-D ordering would appear sooner and even, for $|J'|$ large enough, $\chi_M T$ vs. T would show a constant decrease.

It is actually what happens with compound **5**, containing only three water molecules, as shown in Figure 5. The loss of 4.5 water molecules by binuclear pair, most likely those from the "water bed" between the layers of chains, seems sufficient to break down the 1-D character of the compound; no minimum occurs.

Curve 3 in Figure 5 was attributed in our preliminary note[1] to compound **1**. This curve is, in part, an artifact. It was probably obtained with a partially dehydrated material, intermediate between **1** and **5**. Our initial interpretation about the magnetic ground state has therefore to be revised as proposed in the present paper.

We turn now to the discussion of two theoretical models of the ferrimagnetic chain.

Table VI. Weighted Least-Squares Planes, Atom-to-Plane Distances (10^{-3} Å), and Dihedral Angles (deg) between Planes

	Cu	Ni	Pt
Plane I			
A	−2 (3)	−4 (3)	1 (2)
S(1)	−39 (6)	−17 (5)	−38 (11)
S(2)	45 (6)	25 (5)	35 (13)
S(3)	−42 (6)	−18 (5)	−42 (13)
S(4)	44 (6)	24 (5)	22 (6)
Plane III			
S(1)	−1 (6)	1 (5)	7 (11)
S(2)	1 (6)	−1 (5)	−3 (13)
C1)	18 (19)	−1 (16)	−86 (37)
C(2)	−10 (20)	12 (17)	−20 (40)
O(1)^{i}	1 (13)	−8 (12)	−13 (33)
O(2)^{i}	4 (14)	4 (11)	41 (28)
Plane V			
S(1)	−0 (6)	0 (5)	2 (11)
O(1)^{i}	−3 (13)	0 (12)	18 (33)
C(1)	18 (19)	−2 (16)	−61 (37)
C(2)	−6 (20)	1 (17)	27 (40)
Plane VII			
S(3)	−0 (6)	−0 (5)	−1 (13)
O(3)	1 (14)	−1 (12)	−10 (30)
C(3)	3 (19)	8 (18)	47 (44)
C(4)	−1 (20)	−2 (18)	−12 (37)
Angle			
I–II	4.2	7.4	7.5
I–III	2.1	3.9	2.9
I–IV	2.0	1.3	1.6
II–III	4.9	4.7	5.8
Angles with *b* Axis			
I	89.1	89.5	89.4
II	89.3	89.6	88.6
III	87.0	87.4	87.1
IV	90.6	90.1	90.8

	Cu	Ni	Pt
Plane II			
Mn	−4 (4)	−5 (3)	−14 (8)
O(1)	−94 (13)	−87 (12)	−120 (33)
O(2)	134 (13)	121 (11)	198 (28)
O(3)	62 (14)	66 (12)	103 (29)
O(4)	45 (14)	46 (11)	90 (24)
Ow(3)	−73 (15)	−71 (13)	−87 (31)
Plane IV			
S(3)	1 (6)	5 (5)	1 (13)
S(4)	−0 (6)	−4 (5)	1 (6)
C(3)	−3 (19)	−6 (18)	30 (43)
C(4)	−17 (20)	−14 (18)	−73 (37)
O(3)	−4 (14)	−30 (12)	−5 (30)
O(4)	11 (14)	34 (11)	17 (24)
Plane VI			
S(2)	0 (6)	−0 (11)	0 (13)
O(2)^{i}	2 (14)	−2 (11)	0 (28)
C(1)	4 (19)	−3 (17)	1 (37)
C(2)	−13 (20)	9 (17)	−2 (40)
Plane VIII			
S(4)	0 (6)	0 (5)	1 (6)
O(4)	4 (14)	3 (11)	14 (2)
C(3)	5 (19)	6 (18)	30 (44)
Cn4)	−17 (20)	−21 (18)	−74 (37)
Angle			
II–IV	5.7	6.2	8.4
III–IV	3.8	3.4	4.5
V–VI	0.4	0.5	4.3
VII–VIII	0.7	1.7	1.8

Theory

Until now, no model suitable to predict thermodynamic properties of an alternating chain of spins $S_i = {}^1/_2$ and $S_{i+1} = {}^5/_2$ is available. A closed form expression of the susceptibility of a chain of alternating quantum and classical spins was proposed by Blöte.[22] But, by neglecting spins $^1/_2$ compared to infinite classical spins, a Curie–Weiss law was obtained. The determination of the thermodynamic properties of an infinite system, following the Hamiltonian (3) is, in general, insoluble in an exact manner. With 1-D systems, the problem can be solved by assuming some approximations. We propose two approaches, both involving numerical calculations, whether on rings of alternating quantum spins $^1/_2$ and $^5/_2$ or on an infinite system of alternating quantum spins (copper) and classical ones (manganese).

1. Rings of Alternating Quantum Spins $^1/_2$ and $^5/_2$. We consider a closed ring of N copper–manganese pairs copper(II), spin $^1/_2$, manganese(II), spin $^5/_2$, $\hat{S}_{2N+1} = \hat{S}_1$, and the spin operators $\hat{S}^2$ and $\hat{S}_z$. We define, then, the space of the spin states, $|S, M_S\rangle$ and, for each N, the subspaces corresponding to the different M_S. Eigenvalues are obtained by diagonalizing the Hamiltonian (3) on the basis of these states. There is one (eigen) state with maximum M_S, and Table VII gives the number of states for each M_S for rings with $N = 2, 3, 4$. By successive projections in the subspaces of lower M_S all eigenvalues and the corresponding total spins can be derived. It is then straightforward to use statistical mechanics to obtain the macroscopic properties of the system, as originally proposed by Orbach.[23]

The use of the Hamiltonian (3) involves the following assumptions on the nature of the exchange interaction: the interaction is between nearest neighbors only, the intrachain interaction is isotropic and there is no local zero-field splitting on neither ions, and the interchain interaction is zero.

These points have been already discussed in ref 24.

The thermodynamic properties to be calculated are

$$Z = \sum_{i=1}^{n} (2S_i + 1) \exp(-E_i(S_i)/kT) \qquad (4)$$

(Z is the partition function, E_i is the eigenvalue of eigenstate i,

Table VII. Number of States of Given Positive[a] M_S for Rings of N Pairs of Alternating Quantum Spins $^1/_2$, $^5/_2$

M_S	$N = 2$	$N = 3$	$N = 4$
12			1
11			8
10			32
9		1	88
8		6	192
7		18	360
6	1	38	604
5	4	66	920
4	8	102	1280
3	12	143	1640
2	16	180	1952
1	20	204	2168
0	22	212	2246

[a] Numbers for negative M_S are deduced by symmetry.

(22) Blöte, H. W. J. *J. Appl. Phys.* **1979**, *50*, 7401–7403.
(23) Orbach, R. *Phys. Rev.* **1959**, *115*, 1181–1185.

(24) (a) Verdaguer, M.; Julve, M.; Michalowicz, A.; Kahn, O. *Inorg. Chem.* **1983**, *22*, 2624–2629. (b) The matrix elements were computed by using a home-written Fortran program. The program allows to compute partition function, molar susceptibility in zero field, and specific heat for a given number of pairs of spins S_A and S_B. The maximum order of the matrix which can be handled is 400. Symmetry elements are not taken into account (Verdaguer, M. Thèse d'Etat, Université Paris-Sud, Orsay, 1984).

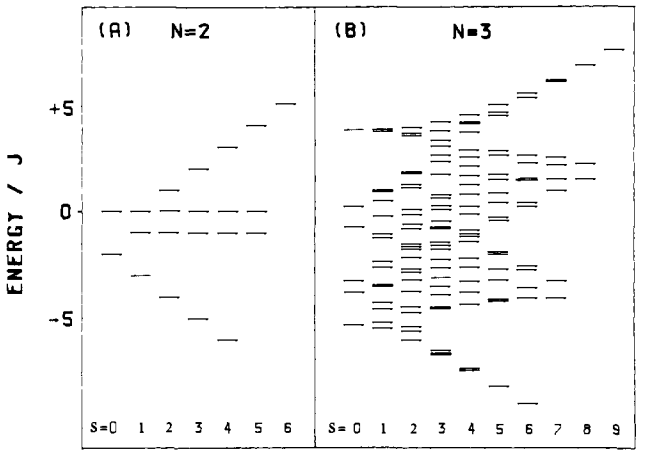

Figure 6. Spectrum of the calculated energy levels and corresponding total spins for (A) a ring of two pairs of quantum spins $^1/_2$, $^5/_2$ ($^1/_2$, $^5/_2$)$_2$ and (B) a ring of three pairs of quantum spins $^1/_2$, $^5/_2$, ($^1/_2$, $^5/_2$)$_3$.

with total spin S_i, E_i is expressed in J units, and n is the number of eigenstates.

$$G = -N_A kT \log Z \tag{5}$$

(G(T,H) is the molar free enthalpy for the magnetic system; k is the Boltzmann constant; N_A is the Avogadro constant).

$$\chi_M = -\frac{N_A \mu_B^2 g^2}{3kT} \sum_{i=1}^{n} \sum_{M_S=-S_i}^{+S_i} M_S^2 \exp(-E_i(S_i)/kT) \frac{1}{Z} \tag{6}$$

(χ_M is the molar susceptibility in zero field, μ_B is the Bohr magneton, and g is a mean value for g factors of copper and manganese).

Calculations have been performed for rings with $N = 2$ and 3. For $N = 4$ we could not perform the calculation[24b] (a 2246th order matrix to diagonalize), and the Bonner–Fisher extrapolation to the thermodynamic limit[25,26] was impossible. Eigenvalues and corresponding spins are given in Figure 6. Variation of $\chi_M T$-$(4/Ng^2)$ vs. $kT/|J|$ is sketched in Figure 7 for an antiferromagnetic interaction. When $kT \gg |J|$ a paramagnetic limit is reached (4.75 cm^3 mol^{-1} K). When $kT \ll |J|$, at the ground state, $S = 2N$, $\chi_M T/N \simeq 2N + 1$. For the infinite chain ($N \to \infty$), $\chi_M T/N$ diverges as $kT/|J|$ tends to zero. For $0.4 \ll kT/|J| < 1.6$, $\chi_M \propto T^{-n}$ with $n \simeq 1.15$ for $N = 2$ and $\simeq 1.33$ for $N = 3$. For intermediate values of $kT/|J|$, the main point is the presence of a minimum (=3.939 cm^3 mol^{-1} K and $kT/|J| = 2.42$ for $N = 2$ and = 3.999 cm^3 mol^{-1} K, and $kT/|J| = 2.85$ for $N = 3$). The minimum can be understood by examination of Figures 6 and 7: leaving the paramagnetic limit by decreasing $kT/|J|$, the first depopulated energy level is the highest; i.e., the one of maximum spin multiplicity, $\chi_M T/N$ decreases. As $\chi_M T/N$ tends to a value higher than that of the paramagnetic limit when $kT/|J|$ tends to zero, there must be a minimum in the curve for intermediate values of $kT/|J|$, in the antiferromagnetic case. For a ferromagnetic interaction, there is no minimum.

The $kT/|J|$ value at the minimum increases with N, but the convergence toward the thermodynamic limit as $N \to \infty$ can be expected to be rather fast.[8,23] In the frame of the assumptions made above, an upper limit of $|J| < 32.3$ cm^{-1} (46.4 K) can be reasonably proposed from the experimental and theoretical values at the minimum.

2. Quantum/Classical Approach. To obtain a better approximation of the value of J, we performed numerical calculations on a quantum/classical proposed elsewhere by Seiden.[13a] The main steps are the following: manganese(II) spins are considered first as classical spins $\vec{S}_i$. The Hamiltonian used is

$$\mathcal{H} = \sum_{i=1}^{N} (\mathcal{H}_u)_i = \sum_{i}^{N} -J[\vec{S}_i + \vec{S}_{i+1}]\vec{s}_i - g\mu_B \vec{H}\left[\frac{\vec{S}_i + \vec{S}_{i+1}}{2} + \vec{s}_i\right] \tag{7}$$

(25) Bonner, J. C.; Fisher, M. E. *Phys. Rev. A* **1964**, *135A*, 640–658.
(26) Bonner, J. C.; Blöte, H. W. J. *Phys. Rev. B* **1982**, *25B*, 6959–6980.

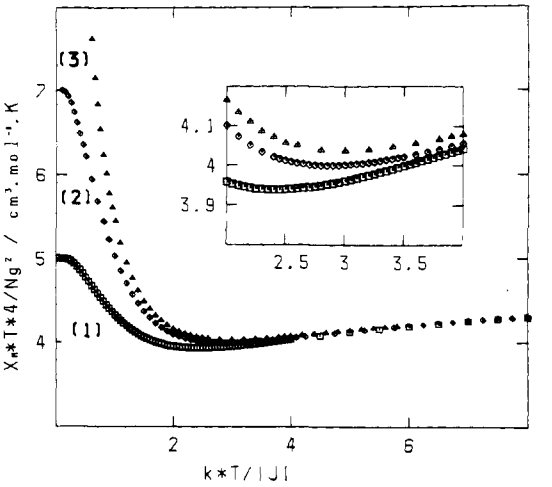

Figure 7. Theoretical $kT/|J|$ dependence of reduced values of $\chi_M T$ ($\chi_M T(4/Ng^2)$) for (1) a ring of two pairs of quantum spins $^1/_2$, $^5/_2$ (curve 1, □), (2) a ring of three pairs of quantum spins $^1/_2$, $^5/_2$ (curve 2, ◇), and (3) a chain of $^1/_2$ quantum spins and alternating classical ones (see text) (curve 3).

where J is the coupling constant between classical spins $\vec{S}_i$ and quantum spins $\vec{s}_i$ in the unit entity u

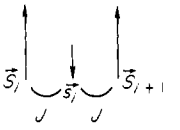

(H is the magnetic field and g is a mean value of g factor for both ions). The main assumption made in this model is that the partition function Z of the system can be obtained by the following relations:

$$Z = \text{trace} \exp(-\mathcal{H}/kT) = \text{trace} (\exp(-\sum_u \mathcal{H}_u/kT)) = \text{trace} \prod_u (\exp(-\mathcal{H}_u/kT)) \tag{8}$$

where the trace operates on all the $\vec{S}_i$ and all the $\vec{s}_i$. $\vec{S}_i$ are classical spins: $\mathcal{H}_u$ relative to different units u commute. The partition function can be written as the trace of a product of factors belonging to the different units u. The trace is then calculated within each unit, first on the quantum spins $\vec{s}$ and then on the manganese ones, using the eigenstates $|Sz\rangle$ of manganese(II), which leads to a sixth order matrix. The thermodynamic properties may be derived, after a matrix transfer treatment, from the highest eigenvalue Λ of this matrix

$$Z = \Lambda^N \tag{9}$$

where N tends to infinity. For small values of H, we have

$$\Lambda = \Lambda_0 + aH^2 \tag{10}$$

it is possible to obtain χ_M from (5), (9), and (10).

$$\frac{\chi_M}{N} = -\frac{\delta^2 G}{\delta H^2} = kT\frac{\delta^2 \log \Lambda}{\delta H^2} \tag{11}$$

We computed Λ_0 and Λ (at $H = 0$ and $10^{-2}kT/g\mu_B$ respectively, when (10) is obeyed). We deduced $\chi_M T(4/Ng^2)$ for each value of $kT/|J|$. The results are sketched in Figure 7 (curve 3): the minimum is at 4.033 cm^3 mol^{-1} K for $kT/|J| = 2.98$. It follows $J = -30.3$ cm^{-1} (43.6 K) and $g = 1.90$.

Mechanism of the Interaction through the Dithiooxalato Bridge in 1. It is well-known that the Heisenberg Hamiltonian is phenomenological: the exchange interaction between paramagnetic centers in a molecular entity is essentially electrostatic in nature.

It is possible, nevertheless, to relate the Heisenberg J coupling constant to the nature and the symmetry of the atoms in the molecule and to express J in terms of fundamental integrals. This has been done in the frame of different models.[2a,b]

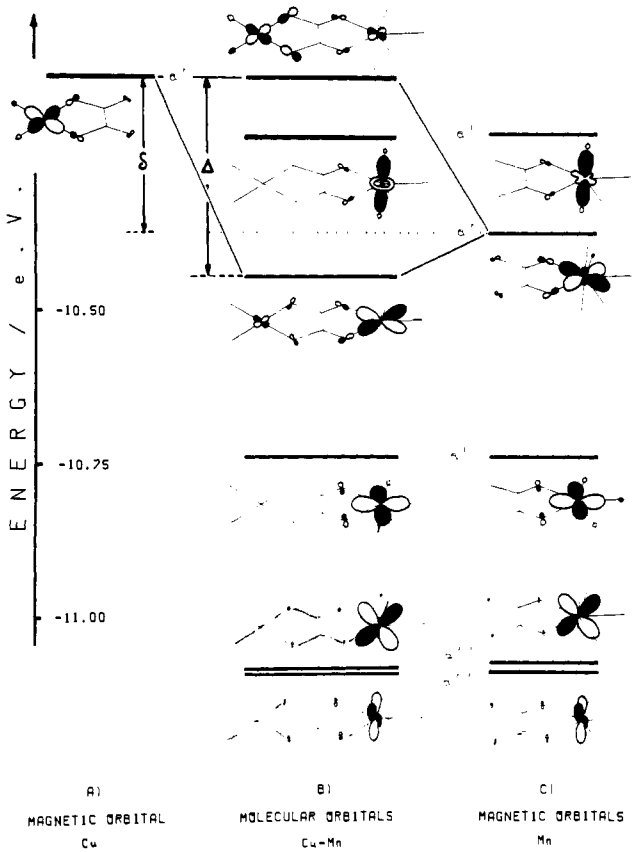

Figure 8. Schematic molecular orbital diagram obtained by extended-Hückel calculations: (A) magnetic orbital around copper(II); (B) molecular orbitals built from magnetic orbitals in the binuclear pair S_2Cu-$S_2C_2O_2MnO_5$; (C) magnetic orbitals around manganese(II).

We propose in this section an orbital interpretation of the exchange, through the dithiooxalato bridge, between copper(II) and manganese(II) ions. We use the orbital model developed by Kahn for homobinuclear[2b] and heterobinuclear complexes[27] and extended to homonuclear chains by Girerd and Charlot.[28] The theory has yet not been achieved for a bimetallic chain. In the following, the chain is considered as a succession of the binuclear pair AB shown in **1**. This unit is roughly planar, with two water

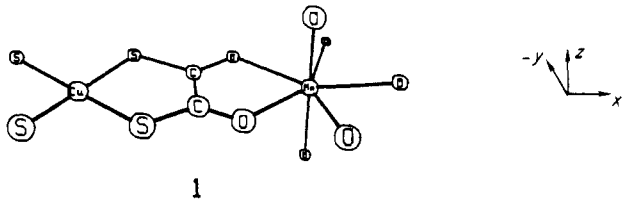

1

molecules binding the manganese(II) ion perpendicularly to the plane of the molecular ribbon. The point symmetry group is very close to C_s, the x axis being along CuMn and the y axis along the CC bond. In the pair AB, there are n_A unpaired electrons and magnetic orbitals (a, symmetry μ: a_μ) and n_B unpaired electrons and magnetic orbitals (b, symmetry ν: b_ν). The copper(II) ion is in a square-planar environment. The magnetic orbital a_μ built from the d_{xy} orbital and partially delocalized toward the sulfur atom has a′ symmetry. The manganese(II) ion is in a pentagonal-bipyramidal arrangement. The five magnetic orbitals b_ν are built from the d_{xy}, d_{z^2}, and $d_{x^2-y^2}$ metallic orbitals (a′ symmetry) and from the d_{xz} and d_{yz} metallic orbitals (a″ symmetry). They are delocalized toward the seven oxygen atoms. The six

Table VIII. Foreseeable Nature and Magnitude of Interaction between Pairs of Magnetic Orbitals of Cu(II) and Mn(II) Ions in a Binuclear Unit of C_s Symmetry

Cu (a_μ)	Mn (b_ν)	$J_{\mu\nu}$	$S_{\mu\nu}$	interaction
xy	xz	$J_{a'a''}$	$\equiv 0$	ferro (weak)
xy	yz	$J_{a'a''}$	$\equiv 0$	ferro (weak)
xy	x^2-y^2	$J_{a'a'}$	$\neq 0$	antiferro (weak)
xy	z^2	$J_{a'a'}$	$\neq 0$	antiferro (weak)
xy	xy	$J_{a'a'}$	$\neq 0$	antiferro (strong)

magnetic orbitals, as obtained by extended-Hückel calculations on the mononuclear fragments[29] are represented in Figure 8. The mixing of manganese(II) d orbitals of the same symmetry is weak, and the simplified model described by Tola[27] can be applied. The coupling constant J is

$$J = \frac{1}{n_A n_B} \sum_\mu \sum_\nu J_{\mu\nu} \tag{12}$$

$J_{\mu\nu}$ corresponds to the different exchange pathways through the bridge. In a first approximation, it is the sum of a positive ferromagnetic contribution arising from interelectronic repulsion (bielectronic integral $j_{\mu\nu}$) and a negative antiferromagnetic contribution arising from monoelectronic integrals and roughly proportional to the square of overlap integral $S_{\mu\nu}$

$$S_{\mu\nu} = \langle a_\mu | b_\nu \rangle \tag{13}$$

$$j_{\mu\nu} = \langle a_\mu(i) b_\nu(j) | r_{ij}^{-1} a_\mu(j) b_\nu(i) \rangle \tag{14}$$

(r_{ij}^{-1} is the interelectronic repulsion energy between electrons i and j at a distance r_{ij}). Table VIII displays the five exchange pathways in the copper–manganese pairs: two of the contributions are ferromagnetic; three are antiferromagnetic, when $S_{\mu\nu} \neq 0$. The ferromagnetic terms, although nonnegligible, are weak since the overlap density $\rho = a_\mu b_\nu$ is small everywhere owing to the polyatomic nature of the ligand.[5] The overlap integrals will govern the antiferromagnetic terms: they are weak for xy/x^2-y^2 and xy/z^2 overlaps but become important for the xy/xy through space overlap between sulfur and oxygen atoms of the dithiooxalato bridge. This σ pathway has already been described for the oxalato bridge.[30] The role of the diffuseness of the p sulfur orbitals has already been pointed out for the dithiooxamido network, explaining a large antiferromagnetic coupling.[31] Extended-Hückel calculations performed on the copper–manganese pair (**1**) confirm these qualitative assumptions.[32] A schematic molecular orbital energy diagram for the magnetic orbitals of the fragments and the molecular orbitals of the pair, with one unpaired electron, is drawn in Figure 8. d_{yz}, d_{xz}, $d_{x^2-y^2}$, and d_{z^2} magnetic orbitals on manganese are almost unchanged whereas d_{xy} magnetic orbitals on copper and manganese distant in energy from $\delta = 0.2505$ eV combine to give two molecular orbitals with an energy gap $\Delta \simeq 0.3317$ eV. This gives rise to a strong antiferromagnetic contribution J_{AF} to $J_{xy/xy}$.[27]

$$J_{AF} \propto (\Delta^2 - \delta^2)^{1/2} \tag{15}$$

The two molecular orbitals obtained in this way are sketched in Figure 8: one of them is stabilized by a bonding interaction between p orbitals of O and S. The antiferromagnetic interaction

(27) Tola, P.; Kahn, O.; Chauvel, C., Coudanne, H. *Nouv. J. Chim.* **1977**, *1*, 467–473.

(28) (a) Girerd, J. J.; Charlot, M. F.; Kahn, O. *Mol. Phys.* **1977**, *34*, 1063–1076. (b) Charlot, M. F.; Girerd, J. J.; Kahn, O. *Phys. Status Solidi B* **1978**, *86*, 497–504.

(29) To obtain the magnetic orbitals we used the FORTICON 8 version of extended-Hückel method, with charge iterations on all atoms and Madelung correction. The mononuclear fragments were $S_2CuS_2C_2O_2$ and $S_2C_2O_2MnO_5$. The geometry was averaged from structural data. The parameters used are given in Appendix I of ref 31a.

(30) Girerd, J. J.; Kahn, O.; Verdaguer, M. *Inorg. Chem.* **1980**, *19*, 274–276.

(31) (a) Girerd, J. J.; Jeannin, S.; Jeannin, Y.; Kahn, O. *Inorg. Chem.* **1978**, *17*, 3034–3040. (b) Chauvel, C.; Girerd, J. J.; Jeannin, Y.; Kahn, O.; Lavigne, G. *Ibid.* **1979** *18*, 3015–3020.

(32) The calculations were performed on the pair, using method zero of the FORTICON 8 program, for the state of maximum spin multiplicity ($S = 3$). The Coulomb integrals used were the corrected H_{ii} issued from the calculations with charge iteration on the mononuclear fragments, the geometry being left unchanged. Results of the calculations must not be overestimated: the quantitative imperfections of the method are well-known. However, a clear qualitative picture of interaction can be gained from them.

experimentally determined, $J = -30.3$ cm^{-1}, sum of various ferromagnetic and antiferromagnetic terms, is therefore essentially determined by the σ-through-space pathway allowed by the xy/xy overlap.

Discussion

We are now in position to give a unified picture of the magnetic properties of compounds **1–5**, in relation to their crystallographic structures. Compounds **1–4** are isostructural: substitution of diamagnetic ions nickel(II) in **2**, palladium(II) in **3**, or platinum(II) in **4** instead of copper(II) in **1** into site A (Figure 1) permits measuring the antiferromagnetic coupling in **2** and **3** and assigning this weak effect to manganese–manganese J' interchain interactions. This seems likely by examining Figure 1: the intrachain manganese–manganese distance is about 12 Å whereas a Mn–OH_2···O–Mn hydrogen pathway appears between two manganese(II) ions at 5.6 Å, belonging to different chains in the same stack of chains. We assume that the same interaction occurs in **1** and that J' can be kept as the interchain interaction in the copper derivative **1**. This implies that there is no or weaker interaction between two CuS_4 groups farther apart than 3.66 Å: as a matter of fact, the staggered configuration of CuS_4 groups (Figure 1) with δ overlap between d_{xy} magnetic orbitals and with a S–S distance larger than the van der Waals distance seems sufficient to hinder a significant interaction. To make sure of this point, it would be of interest to study the susceptibility of an isostructural chain of **1**, where manganese(II) would be substituted by a diamagnetic ion; such synthetic work is in progress.

With this assumption, it is possible to estimate the 1-D character of **1** by computing the ratio of interchain energy $|J|S^2$ upon the intrachain one, $|J|Ss$; this ratio is roughly equal to 0.024. Another way is to reckon the correlation length in the chain from the value of the susceptibility per pair near 3-D ordering: about 20 copper–manganese spins are correlated at 7.9 K.[13a] **1** appears therefore as a rather good 1-D material, where *quasi-1-D ferrimagnetic behavior* has been characterized for the first time. The antiferromagnetic coupling between copper(II) and manganese(II) ions arises from a σ-through-space pathway where the overlap between d_{xy} magnetic orbitals of both ions plays the key role. The dithiooxalato anion, as the oxalato,[30] oxamido and oxamato,[33,34] and dithiooxamido[31] bridges, very efficiently ensures antiferromagnetic coupling between magnetic ions far away from each other.

On the contrary, dehydration of the compound in **5** breaks 1-D behavior by bringing the chains closer together and introducing disorder between the chains and even inside the chains as can be seen from EXAFS measurements at manganese edge:[35] there is no longer a minimum in the $\chi_M T$ vs. T curve for **5** (Figure 5). In the following, we discuss the two theoretical approaches that account for the ferrimagnetic behavior of chain **1**.

The accuracy and the applicability of the quantum rings approach to complex systems are limited by the choice of an isotropic interaction, of a mean value for g, by the restriction to three copper–manganese pairs and to zero magnetic field calculations.

In the quantum-classical approach, it is difficult to appreciate how much the partial transformation of manganese spins to classical ones leads to a significant departure from physical behavior. In Figure 7, the results of both approaches are compared. Curve 3 (quantum classical) is very close to curve 2 (quantum ring of 3 Cu–Mn pairs), calculated with 212 energy levels, distributed over 10 total spin values and an energy band of 16.4 J and which is a rather good approximation of the infinite ring. However, it seems likely that the curve which could be obtained as the thermodynamic limit by the Bonner–Fisher extrapolation[25,26] would be a bit higher than curve 3, in the minimum region, for similar g values.[8,24a]

The fit between experimental and theoretical quantum-chemical approaches shown in Figure 9 is, surprisingly, quite good. The

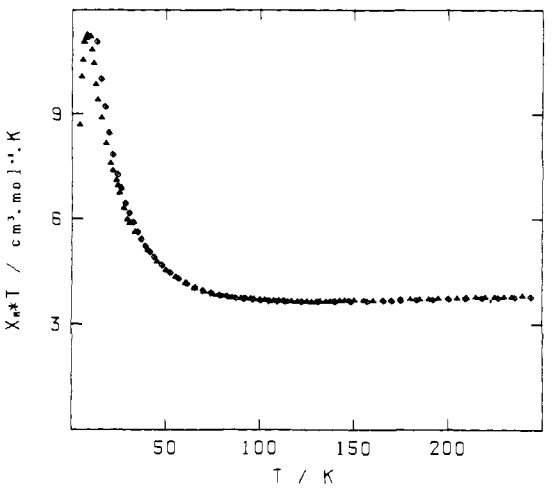

Figure 9. Fitting of the experimental results (△) by the quantum-classical approach (◇, points calculated for $J = -30.3$ cm^{-1} and $g = 1.90$).

1.9 g value, obtained by fitting the minimum of the theoretical and experimental curves seems low and deserves some comments. Recent results[36] on coupled copper(II)–manganese(II) pairs state that, with isotropic g tensors, in the quintuplet state of the pair ($S = 2$), i.e., with typical values, $g_{Mn} = 2.0$, $g_{Cu} = 2.18$, $g_{pair}(S = 2) = 1.97$.

$$g_{pair} = \frac{7}{6}g_{Mn} - \frac{1}{6}g_{Cu} \tag{16}$$

A similar effect leading to a g value less than 2.0 can be expected with a copper–manganese chain, but the theory remains to be done. EPR experiments on this system are at the very beginning and will be reported later.

To verify the J and g values determined at the minimum only, we found that the empirical relation 17 fits very well the quantum-classical curve (curve 3 in Figure 7). ($Y = \chi_M T(4/Ng^2)$; $X = |J|/kT$.)

$$Y = \frac{4.75 - 1.62370X + 2.05042X^2 - 4.52588X^3 - 8.64256X^4}{1 + 0.77968X - 1.56527X^2 - 1.57333X^3 - 0.11666X^{4.5}} \tag{17}$$

Using this empirical relation and allowing g and $|J|$ to vary as adjustable parameters in a least-squares fitting procedure,[37] we found $|J| = 28.3$ cm^{-1} and $g = 1.904$, close to the previous ones. However, uncertainty on the theoretical results leads us to think that the greatest care must be taken in the quantitative estimation of $|J|$ and g.

Conclusion

We synthesized, refined the structures, and studied the magnetic properties of a series of 1-D bimetallic alternating chains $AMn(S_2C_2O_2)_2(H_2O)_3 \cdot 4.5H_2O$ with A = Cu, Ni, Pd, and Pt. The chains are quite well magnetically isolated from each other by intervening water molecules, which permitted the experimental characterization of the quasi-1-D ferrimagnetic behavior of the copper–manganese derivative (**1**). The theoretical models presented fit the experimental data semiquantitatively. We are now engaged in other synthetic, experimental, and theoretical endeavors to specify and to extend our knowledge on this new 1-D ferrimagnetic physical behavior (single-crystal susceptibility mea-

(33) Nonoyama, M.; Nonoyama, K. *J. Inorg. Nucl. Chem.* **1981**, *43*, 2567–2570.
(34) Julve, M.; Verdaguer, M.; Kahn, O., unpublished results.
(35) Verdaguer, M.; Julve, M.; Gleizes, A., work in progress.
(36) (a) Buluggiu, E.; Vera, A. *Z. Naturforsch. A* **1976**, *31A*, 911–914. (b) Buluggiu, E. *J. Phys. Chem. Solids* **1980**, *41*, 1175–1180. (c) Paulson, J. A.; Krost, D. A.; McPherson, G. L.; Rogers, R. D.; Atwood, J. L. *Inorg. Chem.* **1980**, *19*, 2519–2525. (d) Banci, L.; Bencini, A.; Gatteschi, D. *Ibid.* **1981**, *20*, 2734–2735.
(37) A BASIC program based on a Nelder–Mead algorithm (no. 19 in: Nash, J. C. "Compact Numerical Methods for Computers"; Adam Hilger: Bristol, 1979) was used. The reliability factor $R = \sum(y_{obsd} - y_{calcd})^2/\sum(y_{obsd})^2$ was equal to 1.85×10^{-5} for the first fit and to 1.5×10^{-4} for the second fit.
(38) Thermal parameters are available as supplementary material.
(39) Plane equation coefficients are available as supplementary material.

surements, EPR, NMR, heat capacity...). No doubt that beyond this first example of a new class of 1-D, structurally ordered bimetallic compounds, other derivatives synthesized with dissymmetric bridging ligands such as dithiooxalate anion, will enlarge the zoo of exotic magnetic materials and will allow a deeper insight into the chemistry and physics in low dimension.

Acknowledgment. We thank J. Galy, J. P. Renard, and J. Seiden for helpful discussions and O. Kahn for suggesting this exciting area of investigation.

Registry No. 1, 89958-80-5; **2**, 89958-81-6; **3**, 89958-82-7; **4**, 89958-83-8; **5**, 90025-85-7; $K_2Ni(S_2C_2O_2)_2$, 25360-81-0; $K_2Cu(S_2C_2O_2)_2$, 89958-84-9; $K_2Pd(S_2C_2O_2)_2$, 60490-61-1; $K_2Pt(S_2C_2O_2)_2$, 60490-62-2.

Supplementary Material Available: A listing of thermal parameters for atoms of **1** (Table IX) and **2** (Table X), plane equation coefficients for **1**, **2**, and **4** (Table XI), and calculated and observed structure factors for **1** (Table XII) and **2** (Table XIII) (15 pages). Ordering information is given on any current masthead page.

An ab Initio Study of Tautomerism of Uracil, Thymine, 5-Fluorouracil, and Cytosine

Martin J. Scanlan and Ian H. Hillier*

Contribution from the Department of Chemistry, University of Manchester, Manchester M13 9PL, England. *Received October 25, 1983*

Abstract: Geometry optimization using a 3-21G basis has been employed to study the relative energetics of the six tautomers of uracil, thymine, 5-fluorouracil, and cytosine. These calculations yield molecular geometries in good agreement with available experimental data and correctly predict the most stable tautomer of each species. The relative energetics of three tautomers of uracil are predicted in excellent agreement with experiment. Substitution of uracil at the 5-position by CH_3 or F does not change the order of the stabilities of the tautomers. Our results indicate that the tautomeric equilibria of both uracil and cytosine are sensitive to phase change, and it is suggested that at least two and possibly three tautomers of cytosine may be observed in the gas phase. A simple model of solvation is shown to account for the difference in the order of stability of the tautomers of cytosine and uracil in solution and the gas phase.

The relative stability of tautomers of the pyrimidine bases uracil, thymine, and cytosine is of fundamental importance to the structure and functioning of nucleic acids. The occurrence of rare tautomers has been put forward as a possible mechanism of spontaneous mutation. Löwdin[1] and more recently Pullman and Pullman[2] have reviewed the subject comprehensively.

We are here concerned with both lactim–lactam and amine–imine tautomerism.

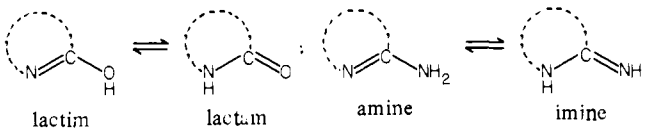

Thus six tautomers of uracil and each of its 5-substituted derivatives thymine and 5-fluorouracil

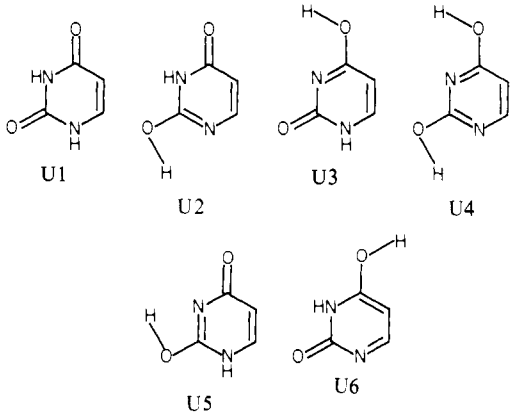

and a further six tautomers of cytosine

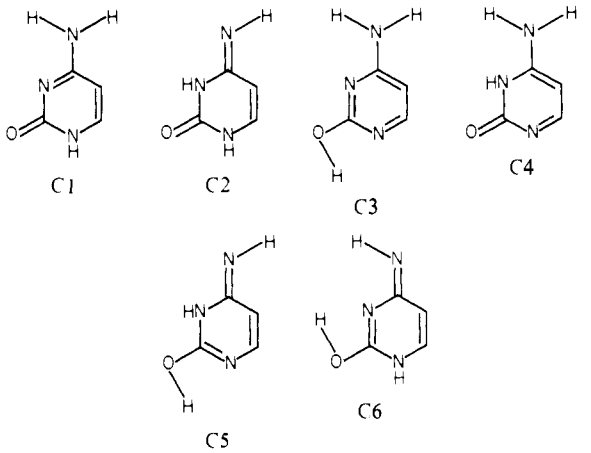

will be considered in this paper. The tautomers of uracil and cytosine are denoted U1–U6 and C1–C6 as shown above. The equivalent tautomers of thymine and 5-fluorouracil are U1–U6 with CH_3 or F substituted at C_5 and will be referred to as T1–T6 and FU1–FU6, respectively.

The dominant tautomer for these bases in both the solid and solution has been conclusively determined to be U1, T1, FU1, and C1.[3] Recently, however, Beak[4,5] has drawn attention to the fact that heterocyclic tautomeric equilibria are highly sensitive to environmental effects such as solvent polarity or transition to the

(1) Löwdin, P. O. *Adv. Quantum. Chem.* **1965**, *2*, 213.
(2) Pullman, B.; Pullman, A. *Adv. Heterocycl. Chem.* **1971**, *13*, 77.
(3) Kwiatkowski, J. S.; Pullman, B. *Adv. Heterocycl. Chem.* **1975**, *18*, 199. For a general discussion of tautomerism in heterocycles, see: Katritzky, A. R.; Linda, P. Ed.; "The Tautomerism of Heterocycles"; Academic Press: New York, 1976; Adv. Heterocycl. Chem., Supplement No. 1.
(4) Beak, P.; Fry, F. S.; Lee, J.; Steele, F. *J. Am. Chem. Soc.* **1976**, *98*, 171.
(5) Beak, P. *Acc. Chem. Res.* **1977**, *10*, 186.

0002-7863/84/1506-3737$01.50/0